12 2D Shape measures for computer vision

PAUL L. ROSIN
School of Computer Science
Cardiff University
Cardiff CF24 3AA, Wales, U.K.
e-mail: Paul.Rosin@cs.cf.ac.uk

JOVIŠA ŽUNIĆ †
Department of Computer Science
University of Exeter
Exeter EX4 4QF, U.K.
e-mail: J.Zunic@ex.ac.uk

12.1 INTRODUCTION

Shape is a critical element of computer vision systems. Its potential value is made more evident by considering how its effectiveness has been demonstrated in biological visual perception. For instance, in psychophysical experiments it was shown that for the task of object recognition, the outline of the shape was generally sufficient, rendering unnecessary the additional internal detail, texture, shading, etc. available in the control photographs [1, 22]. A second example is the so called "shape bias". When children are asked to name new objects, generalising from a set of previously viewed artificial objects, it was found that they tend to generalise on the basis of shape, rather than material, colour, or texture [28, 56].

There are many components in computer vision systems that can use shape information, for example classification [43], shape partitioning [50], contour group-

† J. Žunić is also with the Mathematical Institute, Serbian Academy of Arts and Sciences, Belgrade.

ing [24], removing spurious regions [54], image registration [62], shape from contour [6], snakes [11], image segmentation [31], data mining [64], and content based image retrieval [13], to name just a few.

Over the years many ways have been reported in the literature for describing shape. Sometimes they provide a unified approach that can be applied to determine a variety of shape measures [35], but more often they are specific to a single aspect of shape. This material is covered in several reviews [26, 32, 53, 67] and a comparison of some different shape representations has been carried out as part of the Core Experiment CE-Shape-1 for MPEG-7 [2, 29, 61].

Many shape representations (e.g. moments, Fourier, tangent angle) are capable of reconstructing the original data, possibly up to a transformation (e.g. modulo translation, rotation, scaling, etc). However, for this chapter the completeness of the shape representations is not an issue. A simpler and more compact class of representation in common use is the one dimensional signature (e.g. the histogram of tangent angles). This chapter does not cover such schemes either, but is focused on shape measures that compute single scalar values from a shape. Their advantage is that not only are these measures extremely concise (benefiting storage and matching) but they tend to be designed to be invariant to rotations, translations, and uniform scalings, and often have an intuitive meaning (e.g. circularity) since they describe a single aspect of the shape. The latter point can be helpful for users of computer vision systems to understand their reasoning. The shapes themselves we assume to be extracted from images and are presented either in the form of a set of boundary or interior pixels, or as polygons.

The majority of the measures described have been normalised so that their values lie in the range $[0, 1]$ or $(0, 1]$. Nevertheless, even when measuring the same attribute (e.g. there are many measures of convexity) the values of the measures are not directly comparable since they have not been developed in a common framework (e.g. a probabilistic interpretation).

The chapter is organised as follows: Section 12.2 describes several shape descriptors that are derived by a use of minimum bounding rectangles. The considered shape descriptors are: rectangularity, convexity, rectilinearity, and orientability. Section 12.3 extends the discussion to the shape descriptors that can be derived from other bounding shapes (different from rectangles). Fitting a shape model to the data is a general approach to the measurement of shape; an overview of this is given in Section 12.4. Geometric moments are widely used in computer vision, and their application to shape analysis is described in Section 12.5. The powerful framework of Fourier analysis has also been applied, and Fourier descriptors are a standard means of representing shape, as discussed in Section 12.6.

12.2 MINIMUM BOUNDING RECTANGLES

As we will see in the next section, using a bounding shape is a common method for generating shape measures, but here we will concentrate on a single shape, optimal bounding rectangles, and outline a variety of its applications to shape analysis.

Let $\mathbf{R}(S, \alpha)$ be the minimal area rectangle with edges parallel to the coordinate axes which includes polygon S rotated by an angle α around the origin. Briefly, $\mathbf{R}(S)$ means $\mathbf{R}(S, \alpha = 0)$. Let $\mathbf{R}_{\min}(S)$ be the rectangle that minimises $\mathbf{area}(\mathbf{R}(S, \alpha))$. This can be calculated in linear time with respect to the number of vertices of S by first computing the convex hull followed by Toussaint's [59] "rotating orthogonal calipers" method.

12.2.1 Measuring Rectangularity

There are a few shape descriptors that can be estimated from $\mathbf{R}_{\min}(S)$. For example, a standard approach to measure the rectangularity of a polygonal shape S is to compare S and $\mathbf{R}_{\min}(S)$. Of course, the shape S is said to be a perfectly rectangular shape (i.e. S is a rectangle) if and only if $S = \mathbf{R}_{\min}(S)$. Such a trivial observation suggests that rectangularity can be estimated by:

$$\frac{\mathbf{area}(S)}{\mathbf{area}(\mathbf{R}_{\min}(S))}.$$

Also, the orientation of S can be defined by the orientation of $\mathbf{R}_{\min}(S)$, or more precisely, the orientation of S can be defined by the orientation of the longer edge of $\mathbf{R}_{\min}(S)$. Finally, the elongation of S can be derived from $\mathbf{R}_{\min}(S)$, where the elongation of S is estimated by the ratio of the lengths of the orthogonal edges of $\mathbf{R}_{\min}(S)$.

Analogous measures can be constructed using the minimum perimeter bounding rectangle instead of the minimum area bounding rectangle. Of course, in both cases where the bounding rectangles are used a high sensitivity to the boundary defect is expected.

12.2.2 Measuring Convexity

Curiously, the minimum area bounding rectangle can also be used to measure convexity [70]. Indeed, a trivial observation is that the total sum of projections of all the edges of a given shape S onto the coordinate axes is equal to the Euclidean perimeter of $\mathbf{R}(S)$, which will be denoted by $\mathcal{P}_2(\mathbf{R}(S))$. The sum of projections of all the edges of S onto coordinate axes can be written as $\mathcal{P}_1(S)$, where $\mathcal{P}_1(S)$ means the perimeter of S in the sense of l_1 distance (sometimes called the "city block distance"), and so we have

$$\mathcal{P}_1(S, \alpha) = \mathcal{P}_2(\mathbf{R}(S, \alpha)) \tag{12.1}$$

for every convex polygon S and all $\alpha \in [0, 2\pi)$ ($\mathcal{P}_1(S, \alpha)$ denotes the l_1 perimeter of S after rotation for an angle α).

The equality (12.1) could be satisfied for some non convex polygons, as well (see Fig. 12.1), but a deeper observation (see [70]) shows that for any non convex polygonal shape S there is an angle α such that the strict inequality

$$\mathcal{P}_1(S, \alpha) > \mathcal{P}_2(\mathbf{R}(S, \alpha)) \tag{12.2}$$

holds.

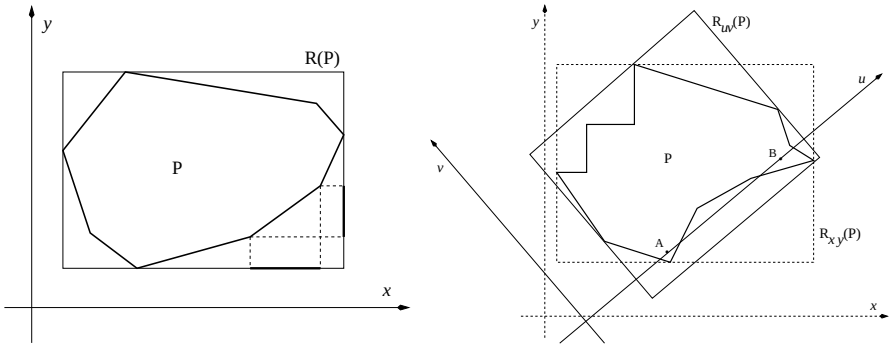

Fig. 12.1 **(a)** Since S is convex then $\mathcal{P}_1(S) = \mathcal{P}_2(\mathbf{R}(S))$. **(b)** If x and y are chosen to be the coordinate axes then $\mathcal{P}_2(\mathbf{R}(S)) = \mathcal{P}_1(S)$. Since S is not convex there is another choice of the coordinate axes, say u and v, such that the strict inequality $\mathcal{P}_2(\mathbf{R}(S)) < \mathcal{P}_1(S)$ holds.

Combining (12.1) and (12.2) the following theorem that gives a useful characterization of convex polygons can be derived.

Theorem 1 *([70]) A polygon S is convex if and only if*

$$\mathcal{P}_1(S, \alpha) = \mathcal{P}_2(\mathbf{R}(S, \alpha))$$

holds for all $\alpha \in [0, 2\pi)$.

Taking into account the previous discussion, the inequality (12.2), and Theorem 1 the following convexity measure $\mathcal{C}(S)$ for a given polygonal shape S is very reasonable:

$$\mathcal{C}(S) = \min_{\alpha \in [0, 2\pi]} \frac{\mathcal{P}_2(\mathbf{R}(S, \alpha))}{\mathcal{P}_1(S, \alpha)}. \tag{12.3}$$

The convexity measure defined as above has several desirable properties:

- The estimated convexity is always a number from $(0, 1]$;
- The estimated convexity is 1 if and only if the measured shape is convex;
- There are shapes whose estimated convexity is arbitrary close to 0;
- The new convexity measure is invariant under similarity transformations.

The minimum of the function $\dfrac{\mathcal{P}_2(\mathbf{R}(S, \alpha))}{\mathcal{P}_1(S, \alpha)}$ that is used to estimate the convexity of a given polygonal shape S cannot be given in a "closed" form. Also, it is obvious that the computation of $\dfrac{\mathcal{P}_2(\mathbf{R}(S, \alpha))}{\mathcal{P}_1(S, \alpha)}$ for a big enough number of uniformly distributed

different values of $\alpha \in [0, 2\pi]$ would lead to an estimate of $\mathcal{C}(S)$ within an arbitrary required precision. But a result from [70] shows that there is a deterministic, very efficient algorithm that enables the exact computation of $\mathcal{C}(S)$. That is an advantage of the method. It turned out that it is enough to compute $\frac{\mathcal{P}_2(\mathbf{R}(S,\alpha))}{\mathcal{P}_1(S,\alpha)}$ for a number of $\mathcal{O}(n)$ different, precisely defined, values of α and take the minimum from the computed values (n denotes the number of vertices of S).

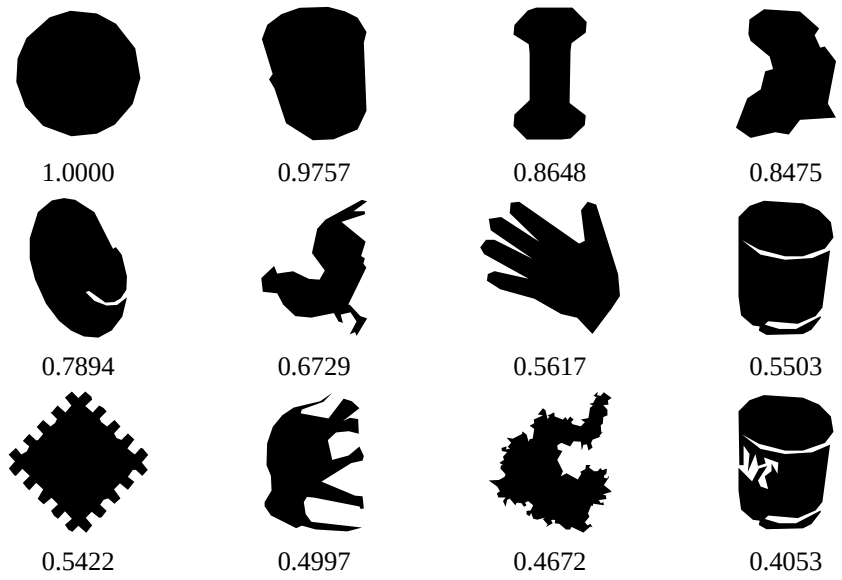

Fig. 12.2 Shapes ranked by the $\mathcal{C}$ convexity measure.

$\mathcal{C}(S)$ is a boundary based convexity measure that implies a high sensitivity to the boundary defects. In the majority of computer vision tasks the robustness (rather than the sensitivity) is a preferred property, but in high precision tasks the priority has to be given to the sensitivity.

Several shapes with their measured convexity values (the convexity measure $\mathcal{C}$ is used) are presented in Fig. 12.2. Each shape S is rotated such that the function $\frac{\mathcal{P}_2(\mathbf{R}(S,\alpha))}{\mathcal{P}_1(S,\alpha)}$ reaches the minimum. The first shape (the first shape in the first row) is convex leading to the measured convexity equal to 1. Since the used measure $\mathcal{C}$ is boundary based, boundary defects are strongly penalized. For example, the first shape in the second row, the last shape in the second row, and the last shape in the third row all have measured convexity values that strongly depend on the intrusions. Also note that there are a variety of different shape convexity measures (e.g. [5, 42, 58]) including both boundary and area based ones.

12.2.3 Measuring Rectilinearity

In addition to the above we give a sketch of two recently introduced shape descriptors with their measures that also use optimal (in a different sense) bounding rectangles. We start with rectilinearity. This shape measure has many possible applications such as shape partitioning, shape from contour, shape retrieval, object classification, image segmentation, skew correction, deprojection of aerial photographs, and scale selection – see [69, 55]. Another application is the detection of buildings from satellite images. The assumption that extracted polygonal areas whose interior angles belong to $\{\pi/2, 3\pi/2\}$ very likely correspond to building footprints on satellite images seems to be reasonable. Consequently, a shape descriptor that would detect how much an extracted region differs from a polygonal area with interior angles belonging to $\{\pi/2, 3\pi/2\}$, could be helpful in detecting buildings on satellite images, (see Fig. 12.3).

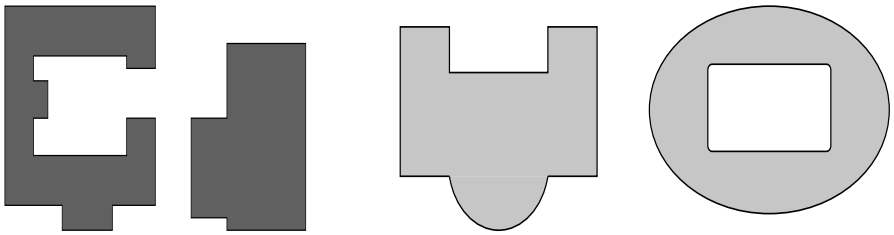

(a) **(b)**

Fig. 12.3 **(a)** The presented rectilinear polygons correspond to building footprints. **(b)** The presented (non-polygonal) shapes correspond to building footprints but they are not rectilinear polygons.

Thus, a shape with interior angles belonging to $\{\pi/2, 3\pi/2\}$ is named a "rectilinear shape", while a shape descriptor that measures the degree to which shape can be described as a rectilinear one is named "shape rectilinearity". It has turned out that the following two quantities

$$\mathcal{R}_1(S) = \frac{4}{4-\pi} \cdot \left(\max_{\alpha \in [0,2\pi)} \frac{\mathcal{P}_2(S)}{\mathcal{P}_1(S,\alpha)} - \frac{\pi}{4} \right) \tag{12.4}$$

$$\mathcal{R}_2(S) = \frac{\pi}{\pi - 2\sqrt{2}} \cdot \left(\max_{\alpha \in [0,2\pi)} \frac{\mathcal{P}_1(S,\alpha)}{\sqrt{2}\mathcal{P}_2(S,\alpha)} - \frac{2\sqrt{2}}{\pi} \right) \tag{12.5}$$

are appropriate to be used as rectilinearity measures. For a detailed explanation see [69]. It is obvious that both $\mathcal{R}_1$ and $\mathcal{R}_2$ are boundary based shape descriptors. An area based rectilinear descriptor is not defined yet. A reasonably good area based rectilinearity measure would be very useful as a building detection tool when working with low quality images.

The following desirable properties of rectilinearity measures $\mathcal{R}_1$ and $\mathcal{R}_2$ hold (for details see [55, 69]):

- Measured rectilinearity values are numbers from $(0, 1]$;
- A polygon S has a measured rectilinearity equal to 1 if and only if S is rectilinear;
- For each $\varepsilon > 0$ there is a polygon whose measured rectilinearity belongs to $(0, \varepsilon)$;
- Measured rectilinearities are invariant under similarity transformations.

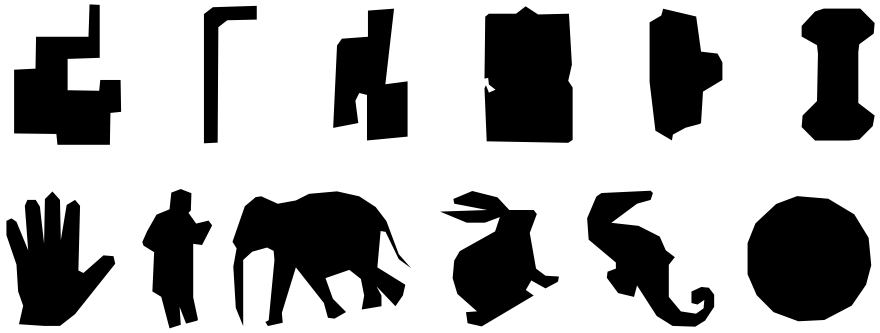

(a) $\mathcal{R}_1$

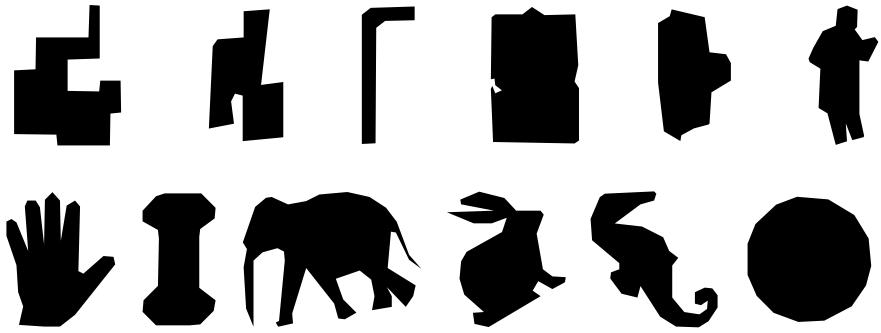

(b) $\mathcal{R}_2$

Fig. 12.4 Shapes ranked by rectilinearity measures $\mathcal{R}_1$ and $\mathcal{R}_2$.

Although $\mathcal{R}_1$ and $\mathcal{R}_2$ are derived from the same source and give similar results, they are indeed different and they could lead to different shape ranking (with respect to the measured rectilinearity). For an illustration see Fig 12.4; shapes presented in Fig 12.4(a) are ranked with respect to $\mathcal{R}_1$ while the shapes presented in Fig 12.4(b) are ranked with respect to $\mathcal{R}_2$.

12.2.4 Measuring Orientability

To close this section on related shape measures based on bounding rectangles we discuss "shape orientability" as a shape descriptor that should indicate the degree to which a shape has a distinct (but not necessarily unique) orientation. This topic was recently investigated by the authors [71]. The definition of the orientability measure uses two optimal bounding rectangles. One of them is the minimum area rectangle $\mathbf{R}_{\min}(S)$ that inscribes the measured shape S while another is the rectangle $\mathbf{R}_{\max}(S)$ that maximizes $\mathbf{area}(\mathbf{R}(S,\alpha))$. A modification of Toussaint's [59] rotating orthogonal calipers method can be used for an efficient computation of $\mathbf{R}_{\max}(S)$. The orientability $\mathcal{D}(S)$ of a given shape S is defined as

$$\mathcal{D}(S) = 1 - \frac{\mathbf{R}_{\min}(S)}{\mathbf{R}_{\max}(S)}. \tag{12.6}$$

Defined as above, the shape orientability has the following desirable properties:

- $\mathcal{D}(S) \in [0,1)$ for any shape S;
- A circle has the measured orientability equal to 0;
- No polygonal shape has the measured orientability equal to 0;
- The measured orientability is invariant with respect to similarity transformations.

Since both $\mathbf{R}_{\min}(S)$ and $\mathbf{R}_{\max}(S)$ are easily computable, it follows that the shape orientability of a given polygonal shape S is also easy to compute. For more details we refer to [71].

Note that a trivial approach could be to measure shape orientability by the degree of elongation of the considered shape. Indeed, it seems reasonable to expect that the more elongated a shape the more distinct its orientation. But if such an approach is used then problems arise with many-fold symmetric shapes, as described later in sections 12.5.1 and 12.5.2. However, measuring shape orientability by the new measure $\mathcal{D}(S)$ is possible in the case of such many-fold symmetric shapes, as demonstrated in Fig. 12.5. This figure gives several trademark examples whose orientability is computed by $\mathcal{D}(S)$. As expected, elongated shapes are considered to be the most orientable. Note however, that the measure $\mathcal{D}(S)$ is also capable of distinguishing different degrees of orientability for several symmetric shapes that have similar compactness, such as the first and last examples in the top row.

12.3 FURTHER BOUNDING SHAPES

The approach taken to measure rectangularity (subsection 12.2.1) can readily also be applied to other shape measures, as long as the bounding geometric primitive can be computed reasonably efficiently. However, in some cases it is not appropriate; for instance sigmoidality (see section 12.4) is determined more by the shape of its medial

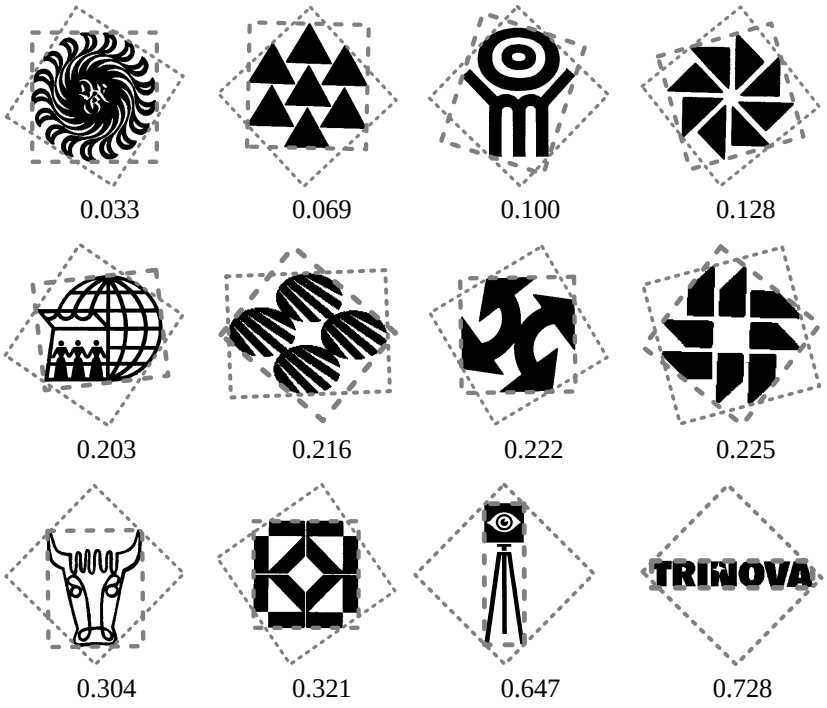

Fig. 12.5 Trademarks ranked by orientability using $\mathcal{D}(S)$. The bounding rectangles $\mathbf{R}_{\min}(S)$ and $\mathbf{R}_{\max}(S)$ are displayed for each measured shape S.

axis than its outline, while other measures such as complexity [40] or elongation (see section 12.5.2) are not defined with respect to any geometric primitive.

A simple and common use of such a method is to measure convexity. If we denote the convex hull of polygon S by $\mathbf{CH}(S)$ then the standard convexity measure is defined as

$$\mathcal{C}_1(S) = \frac{\mathbf{area}(S)}{\mathbf{area}(\mathbf{CH}(S))}.$$

The computation time of the convex hull of a simple polygon is linear in the number of its vertices [36] and so the overall computational complexity of the measure is linear.

A perimeter based version can be used in place of the area based measure:

$$\mathcal{C}_2 = \frac{\mathcal{P}_2(\mathbf{CH}(S))}{\mathcal{P}_2(S)}.$$

It was straightforward to apply the same approach to compute triangularity [51]. Moreover, since linear time (wrt. number of polygon vertices) algorithms are available to determine the minimum area bounding triangle [37, 39] this measure could be computed efficiently. Many other similar measures are possible, and we note

that there are also linear time algorithms available to find bounding circles [18] and bounding ellipses [19] that can be used for estimating circularity and ellipticity.

A more rigorous test of shape is, given a realisation of an ideal shape, to consider fluctuations in both directions, i.e. intrusions and protrusions. Thus, in the field of metrology there is an ANSII standard for measuring roundness which requires finding the minimum width annulus to the data. This involves determining the inscribing and circumscribing circles which have a common centre and minimise the difference in their radii. Although the exact solution is computationally expensive Chan [8] presented an $O(n + \epsilon^{-2})$ algorithm to find an approximate solution that is within a $(1 + \epsilon)$-factor of optimality, where the polygon contains n vertices and $\epsilon > 0$ is an input parameter. We note that in general inscribed shapes are more computationally expensive to compute than their equivalent circumscribing versions (even when the two are fitted independently). For instance the best current algorithm for determining the maximum area empty (i.e. inscribed) rectangle takes $O(n^3)$ time [10] compared to the linear time algorithm for the minimum area bounding rectangle. Even more extreme is the convex skull algorithm; the optimal algorithm runs in $O(n^7)$ time [9] compared again to a linear time algorithm for the convex hull.

12.4 FITTING SHAPES

An obvious scheme for a general class of shape measures is to fit a shape model to the data, and use the goodness of fit as the desired shape measure. There is of course great scope in terms of which fitting procedure is performed, which error measure is used, and the choice of the normalisation of the error of fit.

12.4.1 Ellipse Fitting

For instance, to fit ellipses, Rosin [48] used the Least Median of Squares (LMedS) approach which is robust to outliers, and enables the ellipse to be fitted reliably even in the presence of outliers. The LMedS enables outliers to be rejected, and then a more accurate (and ellipse-specific) least squares fit to the inliers was found [15]. Calculating the shortest distance from each data point to the ellipse requires solving a quartic equation, and so the distances were approximated using the orthogonal conic distance approximation method [47]. The average approximated error over the data E was combined with the region's area A to make the ellipticity measure scale invariant [51]:

$$\left(1 + \frac{E}{\sqrt{A}}\right)^{-1}.$$

12.4.2 Triangle Fitting

For fitting triangles a different approach was taken. The optimal three line polygonal approximation that minimised the total absolute error to the polygon was found using

dynamic programming. The average error was then normalised as above to give a triangularity measure [51].

12.4.3 Rectangle Fitting

An alternative approach to measure rectangularity [51] from the one introduced in section 12.2 is to iteratively fit a rectangle R to S by maximising the functional

$$1 - \frac{\mathbf{area}(R \setminus S) + \mathbf{area}(S \setminus R)}{\mathbf{area}(S \cap R)}. \tag{12.7}$$

based on the two set differences between R and S normalised by the union of R and S. This provides a trade-off between forcing the rectangle to contain most of the data while keeping the rectangle as small as possible, as demonstrated in Fig. 12.6. Each iteration can be performed in $O(n \log n)$ time [12], where n is the number of vertices.

(a) (b)

Fig. 12.6 The rectangle shown in (a) was fitted according to (12.7) as compared to the minimum bounding rectangle shown in (b).

12.4.4 Sigmoid Fitting

To measure sigmoidality (i.e. how much a region is S-shaped) several methods were developed that analyse a single centreline curve which was extracted from the region by smoothing the region until the skeleton (obtained by any thinning algorithm) is non-branching. The centreline is then rotated so that its principal axis lies along the x-axis. Fischer and Bunke [14] fitted a cubic polynomial $y = ax^3 + bx^2 + cx + d$ and classified the shape into linear, C-shaped, and sigmoid classes based on the coefficient values. A modified version specifically designed to produce only a sigmoidality measure [52] fitted the symmetric curve given by $y = ax^3 + bx + c$. The correlation coefficient ρ was used to measure the quality of fit between the data and the sampled model. Inverse correlation was not expected, and so the value was truncated at zero.

Rather than fit models directly to the coordinates other derived data can be used instead. The following approach to compute sigmoidality used the tangent angle which was modelled by a Generalised Gaussian distribution [52] – see Fig. 12.7. The

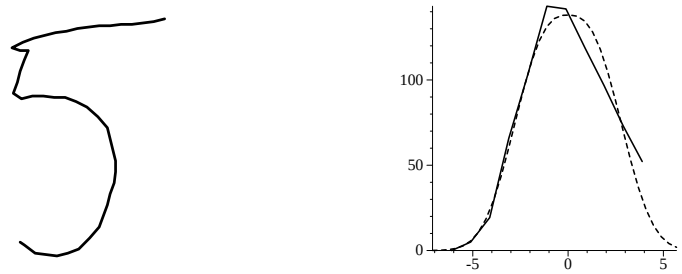

Fig. 12.7 The tangent angle of the handwritten digit '5' is overlaid with the best fit Generalised Gaussian (dashed) – the good fit yields a high sigmoidality measure.

probability density function is given by

$$p(x) = \frac{v\eta(v,\sigma)}{2\Gamma(1/v)} e^{-[\eta(v,\sigma)|x|]^v}$$

where $\Gamma(x)$ is the gamma function, σ is the standard deviation, v is a shape parameter controlling the peakiness of the distribution (values $v = 1$ and $v = 2$ correspond to Laplacian and Gaussian densities), and the following is a scaling function

$$\eta(v,\sigma) = \frac{1}{\sigma}\sqrt{\frac{\Gamma(3/v)}{\Gamma(1/v)}}.$$

Mallat's method [34] for estimating the parameters was employed. First the mean absolute value and variance of the data x_i are matched to the Generalised Gaussian. If $m_1 = \frac{1}{n}\sum_{i=1}^{n}|x_i|$ and $m_2 = \frac{1}{n}\sum_{i=1}^{n}x_i^2$ then

$$v = F^{-1}\left(\frac{m_1}{\sqrt{m_2}}\right)$$

where

$$F(\alpha) = \frac{\Gamma(2/\alpha)}{\sqrt{\Gamma(1/\alpha)\Gamma(3/\alpha)}}.$$

In practise, values of $F(\alpha)$ are precomputed, and the inverse function determined by a look-up table with linear interpolation. Finally, the tangent angle is scaled so that the area under the curve sums to one. It was found that rather then calculating the measure as the correlation coefficient better results were obtained by taking the area of intersection A of the curves as an indication of the error of fit. An approximate normalisation was found by experimentation as $\max(2A - 1, 0)$.

12.4.5 Using Circle and Ellipse Fits

Koprnicky *et al.* [27] fitted two model shapes M (a circle and ellipse) to the data S and for each considered four different error measures: the outer difference

$$\frac{\mathbf{area}(S \cap \overline{M})}{\mathbf{area}(S)},$$

the inner difference

$$\frac{\mathbf{area}(\overline{S} \cap M)}{\mathbf{area}(S)},$$

as well as the sum and difference of the above. This provided four different measures, from which the first three can be considered as circularity and ellipticity measures, focussing on the different aspects of the errors.

12.5 MOMENTS

Moments are widely used in shape analysis tasks. Shape normalization, shape encoding (characterization), shape matching and shape identification are just some examples where moments techniques are successfully applied. To be precise, by "shape moments" we mean geometric moments. The geometric moment $m_{p,q}(S)$ of a given planar shape S is defined by

$$m_{p,q}(S) = \iint_S x^p y^q \, dxdy.$$

In real image processing applications we are working with discrete data resulting from a particular digitization process applied to real data. In the most typical situation real objects are replaced with a set of pixels whose centres belong to the considered shape. In such a case the exact computation of geometric moments is not possible and each used moment $m_{p,q}(S)$ is usually replaced with its discrete analogue $\mu_{p,q}(S)$ which is defined as

$$\mu_{p,q}(S) = \sum_{(i,j) \in S \cap \mathbf{Z}^2} i^p j^q,$$

where $\mathbf{Z}$ means the set of integers. The order of $m_{p,q}(S)$ is said to be $p + q$. Note that the zeroth order moment $m_{0,0}(S)$ of a shape S coincides with the area of S.

12.5.1 Shape Normalization: Gravity Centre and Orientation

Shape normalization is usually an initial step in image analysis tasks or a part of data preprocessing. It is important to provide an efficient normalization because a significant error in this early stage of image analysis would lead to a large cumulative error at the end of processing.

Shape normalization starts with the computation of image position. A common approach is that the shape position is determined by its gravity centre (i.e. centre of mass or, simply, centroid) of a given shape. Formally, for a given planar shape S its gravity centre $(x_c(S), y_c(S))$ is defined as a function of the shape area (i.e., the zeroth order moment of the shape) and the first order moments

$$(x_c(S), y_c(S)) = \left(\frac{m_{1,0}(S)}{m_{0,0}(S)}, \frac{m_{0,1}(S)}{m_{0,0}(S)} \right). \tag{12.8}$$

Computation of shape orientation is another step in the shape normalization procedure which is computed using moments. The orientation seems to be a very natural feature for many shapes, although obviously there are some shapes that do not have a distinct orientation. Many rotationally symmetric shapes are shapes that do not have a unique orientation while the circular disc is a shape that does not have any specific orientation at all. The standard approach defines the shape orientation by a line that minimizes the integral of the squared distances of points (belonging to the shape) to this line. Such a line is also known as the "axis of the least second moment of inertia". If $r(x, y, \delta, \rho)$ denotes the perpendicular distance from the point (x, y) to the line given in the form

$$x \cos \delta - y \sin \delta = \rho$$

then the integral that should be minimized is

$$I(\delta, \rho, S) = \iint_S r^2(x, z, \delta, \rho) dx dy.$$

Elementary mathematics shows that the line which minimizes $I(\delta, \rho, S)$ passes through the centroid $(x_c(S), y_c(S))$ of S and consequently we can set $\rho = 0$. Thus, the problem of orientation of a given shape S is transformed to the problem of computing the angle δ for which the integral

$$I(\delta, S) = \iint_S (-x \sin \delta + y \cos \delta)^2 dx dx \tag{12.9}$$

reaches the minimum. Finally, if we introduce central geometric moments $\overline{m}_{p,q}(S)$ defined as usual

$$\overline{m}_{p,q}(S) \iint_S (x - x_c(S))^2 (y - y_c(S))^2 dx dy$$

then the function $I(\delta, S)$ can be written as

$$I(\delta, S) = \overline{m}_{2,0}(S)(\sin \delta)^2 - 2\overline{m}_{1,1}(S) \sin \delta \cos \delta + \overline{m}_{0,2}(S)(\cos \delta)^2 \tag{12.10}$$

i.e. as a polynomial in $\cos \delta$ and $\sin \delta$ whose coefficients are the second order moments of S. The angle δ for which $I(\delta, S)$ reaches its maximum defines the orientation of S.

Such an angle δ is easy to compute and it can be derived that the required δ satisfies the equation

$$\frac{\sin(2\delta)}{\cos(2\delta)} = \frac{2\overline{m}_{1,1}(S)}{\overline{m}_{2,0}(S) - \overline{m}_{0,2}(S)}. \tag{12.11}$$

It is worth mentioning that if working in discrete space, i.e., if continuous shapes are replaced with their digitizations, then real moments have to be replaced with their discrete analogues. For example, the orientation of discrete shape that is the result of digitization of S is defined as a solution of the following optimization problem

$$\min_{\delta\in[0,2\pi)} \left\{ \sum_{(i,j)\in S\cap\mathbf{Z}^2} (i\sin\delta - j\cos\delta)^2 \right\}.$$

The angle δ which is a solution of the above problem satisfies the equation

$$\frac{\sin(2\delta)}{\cos(2\delta)} = \frac{2\overline{\mu}_{1,1}(S)}{\overline{\mu}_{2,0}(S) - \overline{\mu}_{0,2}(S)}$$

which is an analogue to (12.11).

So, the shape orientation defined by the axis of the least second moment of inertia is well motivated and easy to compute in both continuous and discrete versions. As expected, there are some situations when the method does not give any answer as to what the shape orientation should be. Such situations, where the standard method cannot be applied are characterised by

$$I(\delta, S) = constant. \tag{12.12}$$

There are many regular and irregular shapes that satisfy (12.12). The result from [60] says that (12.12) holds for all N-fold rotationally symmetric shapes with $N > 2$, where N-fold rotationally symmetric shapes are such shapes which are identical to themselves after being rotated through any multiple of $2\pi/N$.

In order to expand the class of shapes with a computable orientation Tsai and Chou [60] suggested a use of the so called N-th order central moments $I_N(\delta, S)$. For a discrete shape S those moments are defined by

$$I_N(\delta, S) = \sum_{(x,y)\in S} (-x\sin\delta + y\cos\delta)^N \tag{12.13}$$

assuming that the centroid of S is coincident with the origin.

Now, the shape orientation is defined by the angle δ for which $I_N(\delta, S)$ reaches the minimum. For $N = 2$ we have the standard method. Note that $I_N(\delta, S)$ is a polynomial in $\cos\delta$ and $\sin\delta$ while polynomial coefficients are central moments of S having the order less or equal to N.

A benefit from this redefined shape orientation is that the method can be applied to a wider class of shapes. For example, since a square is a 4-fold rotationally symmetric shape the standard method does not work. If $I_4(\delta, S)$ is used then the square can be

oriented. A disadvantage is that there is not a closed formula (as (12.11)) that gives δ for which $I_N(\delta, S)$ reaches the minimum for an arbitrary shape S. Thus, a numerical computation has to be applied in order to compute shape orientation in the modified sense.

Fig. 12.8 displays some shapes whose orientation is computed by applying the standard method ($N = 2$) and by applying the modified method with $N = 4$ and $N = 8$. Shapes **(1)**, **(2)**, and **(3)** are not symmetric, but they have a very distinct orientation. Because of that all three measured orientations are almost identical. Shapes **(4)**, **(5)**, and **(6)** have exactly one axis of symmetry and consequently their orientation is well determined. That is the reason why all three computed orientations coincide. The small variation in the case of the bull sketch (shape **(5)**) is caused by the fact that the sketch contains a relatively small number of (black) pixels, and consequently the digitization error has a large influence. Shapes **(7)**, **(8)**, **(9)**, and **(10)** do not have a distinct orientation. That explains the variation in the computed orientations. For shapes **(11)** and **(12)** the standard method does not work. The presented regular triangle is a 3-fold rotationally symmetric shape and its orientation cannot be computed for $N = 4$, as well. For $N = 8$ the computed orientation is 150° which is very reasonable. This is the direction of one of the symmetry axes. Of course, the modified method (in the case of $N = 8$) gives the angles $\delta = 270^\circ$ and $\delta = 30^\circ$ as the minimum of the function $I_8(\delta, S)$ and those angles can be also taken as the orientation of the presented triangle. The last shape is a 4-fold rotationally symmetric shape whose orientation cannot be computed by the standard method.

12.5.2 Shape Elongation

Shape elongation is another shape descriptor with a clear intuitive meaning. A commonly used measure of elongatedness uses the central moments and is computed as the ratio of the maximum of $I(\delta, S)$ and the minimum of $I(\delta, S)$; i.e. shape elongation is measured as ([38])

$$\frac{\overline{\mu}_{20}(S) + \overline{\mu}_{02}(S) + \sqrt{(\overline{\mu}_{20}(S) - \overline{\mu}_{02}(S))^2 + 4\overline{\mu}_{11}(S)^2}}{\overline{\mu}_{20}(S) + \overline{\mu}_{02}(S) - \sqrt{(\overline{\mu}_{20}(S) - \overline{\mu}_{02}(S))^2 + 4\overline{\mu}_{11}(S)^2}}, \tag{12.14}$$

which can be simplified and reformulated as

$$\frac{\sqrt{(\overline{\mu}_{20}(S) - \overline{\mu}_{02}(S))^2 + 4\overline{\mu}_{11}(S)^2}}{\overline{\mu}_{20}(S) + \overline{\mu}_{02}(S)}$$

to provide a measure in the range $[0, 1]$.

Similarly as in the previous subsection some problems arise when working with shapes satisfying $I(\delta, S) = constant$. All such shapes have the same measured elongation equal to 1. Rather, it is more reasonable that all the regular $2n$-gons have the same measured elongation. It seems natural that the elongation of regular $2n$-gons decreases if n increases. Partially, the problem can be avoided if higher order moments of inertia are used. A possibility (see [68]) is to define the elongation of a

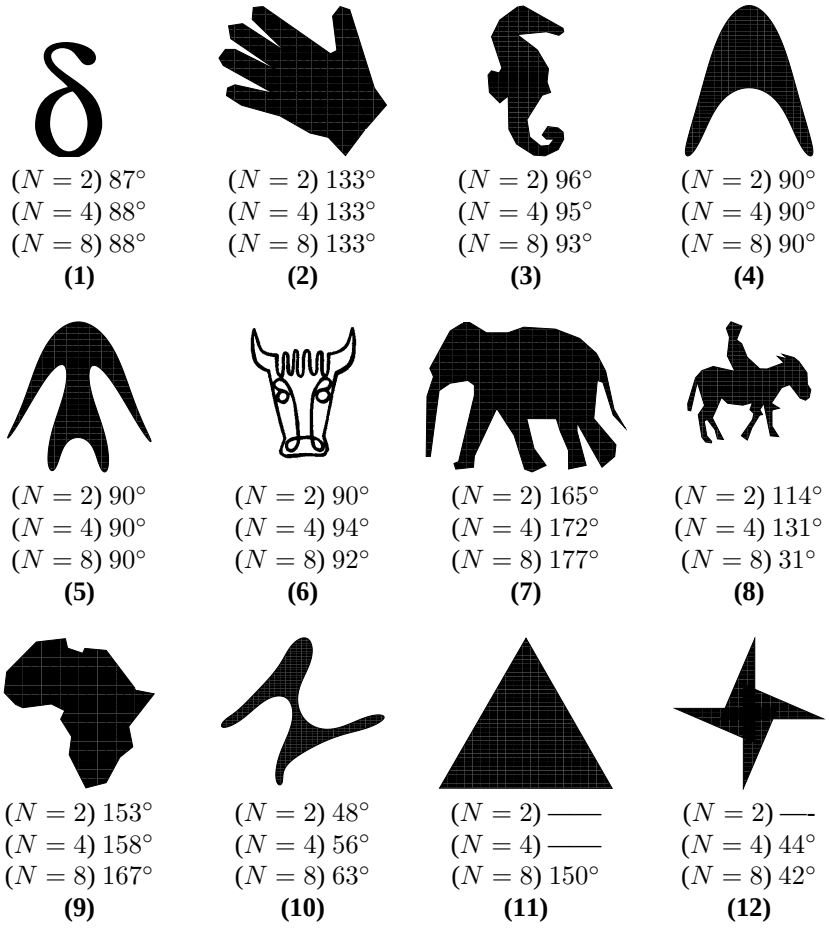

Fig. 12.8 Computed orientation of the presented shapes for $N = 2$, $N = 4$, and $N = 8$ are given (in degrees).

given shape S as

$$\frac{\max\{I_N(\delta, S) \mid \delta \in [0, 2\pi)\}}{\min\{I_N(\delta, S) \mid \delta \in [0, 2\pi)\}}. \tag{12.15}$$

Again, an advantage of the modified definition of the shape orientation is that a smaller class of shapes would have the measured elongation equal to 1. Such the minimum possible measured elongation should be reserved for the circular disc only. On the other hand, for $N > 2$ there is no closed formula (like (12.14)) that can be used for immediate computation of the shape elongation. More expensive numerical

algorithms have to be applied. For more details about elongation of many-fold rotationally symmetric shapes see [68].

12.5.3 Other Shape Measures

A simple scheme for measuring rectangularity [49] considers the moments of a rectangle (dimensions $a \times b$) centred at the origin and aligned with the axes. The moments are $m_{00} = ab$ and $m_{22} = \frac{a^3b^3}{144}$, and so the quantity

$$R = 144 \times \frac{m_{22}}{m_{00}^3}$$

is invariant for rectangles of variable aspect ratio and scaling, and can be normalised as

$$R_M = \begin{cases} R & \text{if } R \leq 1 \\ \frac{1}{R} & \text{otherwise.} \end{cases}$$

To add invariance to rotation and translation the data is first normalised in the standard way by moving its centroid to the origin and orienting its principal axis to lie along the X-axis.

A straightforward scheme to measure similarity to shapes such as triangles and ellipses which do not change their category of shape under affine transformations is to use affine moment invariants [51]. The simplest version is to characterise shape using just the first, lowest order affine moment invariant [16]

$$I_1 = \frac{\overline{m}_{20}\overline{m}_{02} - \overline{m}_{11}^2}{\overline{m}_{00}^4}.$$

This has the advantage that it less sensitive to noise than the higher order moments. The moments for the unit radius circle are

$$\mu_{pq} = \int_{-1}^{1} \int_{-\sqrt{r^2-x^2}}^{\sqrt{r^2-x^2}} x^p y^q dy dx$$

leading to the value of its invariant as $I_1 = \frac{1}{16\pi^2}$. When normalised appropriately this then provides a measure of ellipticity

$$E_I = \begin{cases} 16\pi^2 I_1 & \text{if } I_1 \leq \frac{1}{16\pi^2} \\ \frac{1}{16\pi^2 I_1} & \text{otherwise} \end{cases}$$

which ranges over $[0, 1]$, peaking at 1 for a perfect ellipse. The same approach was applied to triangles, all of which have the value $I_1 = \frac{1}{108}$, and the triangularity

measure is

$$T_I = \begin{cases} 108 I_1 & \text{if } I_1 \leq \frac{1}{108} \\ \dfrac{1}{108 I_1} & \text{otherwise} \end{cases} .$$

Of course, using a single moment invariant is not very specific, and so the above two measures will sometimes incorrectly assign high ellipticity or triangularity values to some other non-elliptical or triangular shapes. This can be remedied using more moment values, either in the above framework, or as described next.

Voss and Süße describe a method for fitting geometric primitives by the method of moments [63]. The data is normalised into a (if possible unique) canonical frame, that is generally defined as the simplest instance of each primitive type, by applying an affine transformation. Applying the inverse transformation to the primitive produces the fitted primitive. For example, for an ellipse they take the unit circle as the canonical form, and the circle in the canonical frame is transformed back to an ellipse, thereby providing an ellipse fit to the data. For the purposes of generating shape measures the inverse transformation is not necessary as the measures can be calculated in the canonical frame. This is done by computing the differences between the normalised moments of the data (m'_{ij}) and the moments of the canonical primitive (m_{ij}) where only the moments not used to determine the normalisation are included:

$$\left(1 + \sum_{i+j \leq 4} (m'_{ij} - m_{ij})^2 \right)^{-1} .$$

The above approach method was applied in this manner by Rosin [51] to generate measures of ellipticity and triangularity. Measuring rectangularity can be done in the same way, except that for fitting rectangles the procedure is modified to apply a similarity transformation rather than an affine transformation. After this transformation the rectangle's aspect ratio remains to be determined, and this is done by a one-dimensional optimisation using the higher order moments (up to fourth order).

We note that the above methods can all compute the moments either from the polygon boundary directly (line moments) [57] or else can operate on the rasterized set of pixels inside the polygon (region) [33].

12.6 FOURIER DESCRIPTORS

Like moments, Fourier descriptors are a standard means of representing shape. This involves taking a Fourier expansion of the boundary function, which itself may be described in a variety of ways. If the boundary of the region is given by the points (x_j, y_j); $j = 1 \ldots N$ then one approach is to represent the coordinates by complex numbers $z_j = x_j + iy_j$ [21]. Other possibilities are to represent the boundary by real 1D functions versus arc length such as tangent angle [66] or radius from the centroid.

Taking the representation $z_j = x_j + iy_j$ and applying the discrete Fourier transform leads to the complex coefficients which make up the descriptors

$$F_k = a_k + ib_k = \frac{1}{N}\sum_{m=0}^{N-1} z_m \exp(-i2\pi mk/N).$$

Often just the magnitude is used $r_k = \sqrt{a_k^2 + b_k^2}$, and since r_1 indicates the size of the region it can be used to make the descriptors scale invariant: $w_k = r_k/r_1$.

For a study of sand particles Bowman *et al.* [4] used individual Fourier descriptors to describe specific aspects of shape, e.g. w_{-3}, w_{-2}, w_{-1} and w_{+1} to measure respectively squareness, triangularity, elongation, and asymmetry. However, this approach is rather crude. A modification [53] to make the measure more specific includes the relevant harmonics and also takes into account the remaining harmonics which do not contribute to squareness:

$$(w_{-3} + w_{-7} + w_{-11} + \ldots)/\sum_{\forall i \notin \{-1,0,1\}} w_i.$$

Kakarala [25] uses the same boundary representation and derives the following expression for the Fourier expansion of the boundary curvature

$$K_n = \frac{1}{2}\sum_{m=-N}^{N} m\left[(m+n)^2\overline{F_m}F_{m+n} + (m-n)^2 F_m\overline{F_{m-n}}\right]$$

where $\overline{F}$ is the complex conjugate of F.

He shows that for a convex contour

$$K_0 \geq 2\sum_{n=1}^{2N}|K_n|$$

from which the following convexity shape measure is derived

$$\frac{K_0 - 2\sum_{n=1}^{2N}|K_n|}{\sum_{n=-2N}^{2N}|K_n|}.$$

Another measure based on curvature is "bending energy" which considers the analogue of the amount of energy required to deform a physical rod [65]. If a circle (which has minimum bending energy) is considered to be the simplest possible shape, then bending energy can be interpreted as a measure of shape complexity or deviation from circularity.

The normalised energy is the summed squared curvature values along the boundary, which can be expressed in the Fourier domain as

$$\sum_{m=-N}^{N} \left(\frac{2\pi m}{N}\right)^4 \left(|a_m|^2 + |b_m|^2\right)$$

although in practice the authors performed the computation in the spatial domain.

When the boundary is represented instead by the radius function a "roughness coefficient" can be defined as

$$\sqrt{\frac{1}{2} \sum_{n=1}^{[(N+1)/2]-1} (a_n^2 + b_n^2)}.$$

This shape measure is effectively the mean squared deviation of the radius function from a circle of equal area [26].

12.7 CONCLUSIONS

This chapter has described several approaches for computing shape measures, and has showed how each of these can then be applied to generate a variety of specific shape measures such as convexity, rectangularity, etc. Fig. 12.9 illustrates some of the geometric primitives that have been inscribed, circumscribed, or otherwise fitted to example data, and which are then used to generate shape measures.

Our survey is not complete, as there exist some methodologies in the literature that we have not covered. Here, for instance, *Information Theory* has been used to measure convexity [41] and complexity [40, 44, 17]. *Projections* are a common tool in image processing, and in the context of the Radon transform have also been used to compute convexity, elongation, and angularity shape measures [30]; a measure of triangularity was also based on projections [51]. Only a brief mention has been made to the issues of digitisation, but it is important to note that this can have a significant effect. For instance, the popular compactness measure $\frac{\mathcal{P}_2(S)^2}{\mathbf{area}(S)}$ in the continuous domain is minimised by a circle but this is not true when working with digital data [45]. Therefore, some measures explicitly consider the digitisation process. e.g. for convexity [46], digital compactness [7, 3] and other shape measures [20].

Given these methodologies it should be reasonably straightforward for the reader to construct new shape measures as necessary. For instance, consider an application requiring a "pentagonality" measure, i.e. the similarity of a polygon to a regular pentagon. Considering the various methods discussed in this chapter, several seem to be readily applicable:

- a measure could be generated from the polygon's bounding pentagon, see section 12.3,

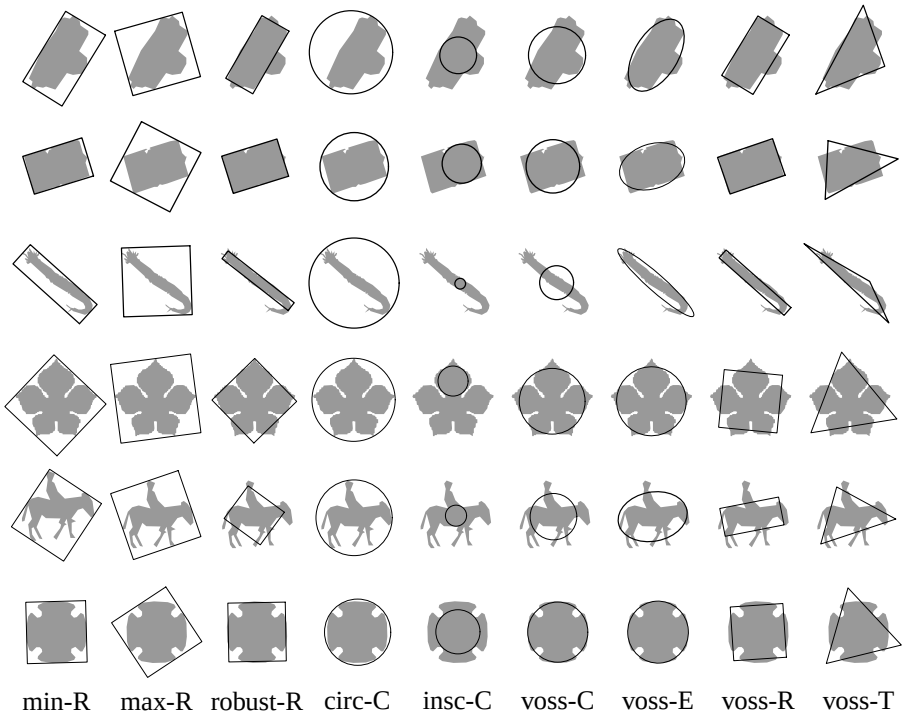

Fig. 12.9 Geometric primitives fitted to shapes. min-R: minimum area rectangle; max-R: maximum area rectangle; robust-R: best fit rectangle – eqn (12.7); circ-C: circumscribing circle; insc-C: inscribed circle; voss-C, voss-E, voss-R, voss-T: circle, ellipse, rectangle and triangle fitted by Voss and Süße's moment based method [63]. These primitives are used to generate some of the shape measures described in this chapter.

- once a pentagon is fitted to the polygon's coordinates various shape measures can be produced, see section 12.4,
- rather than directly processing the polygon's coordinates the histogram of boundary tangents could be used instead, and it would be straightforward to fit fit five regular peaks and then compute a shape measure from the error of fit, see again section 12.4,
- the two methods for generating shape measures from moments by Voss and Süße [63] and Rosin [51] could readily be applied, see section 12.5.3,
- the Fourier descriptor method for calculating triangularity in section 12.6 could also be readily adapted to computing pentagonality.

The natural question is, which is the best shape measure? While measures can be rated in terms of their computational efficiency, sensitivity to noise, invariance to transformations, and robustness to occlusion, ultimately their effectiveness depends on their application. For example, whereas for one application reliability in the

presence of noise may be vital, for another sensitivity to subtle variations in shape may be more important. It should also be noted that, while there are many possible shape measures already available in the literature, and many more that can be designed, they are not all independent. Some analysis on this topic was carried out by Hentschel and Page [23] who computed the correlations between many similar measures as well as determining the most effective for the specific task of powder particle analysis.

References

1. I. Biederman and G. Ju. Surface versus edge-based determinants of visual recognition. *Cognitive Psychology*, 20:38–64, 1988.

2. M. Bober. MPEG-7 visual shape descriptors. *IEEE Trans. Circuits Syst. Video Techn.*, 11(6):716–719, 2001.

3. J. Bogaert, R. Rousseau, P. Van Hecke, and I. Impens. Alternative area-perimeter ratios for measurement of 2D-shape compactness of habitats. *Applied Mathematics and Computation*, 111:71–85, 2000.

4. E.T. Bowman, K. Soga, and T. Drummond. Particle shape characterization using Fourier analysis. *Geotechnique*, 51(6):545–554, 2001.

5. L. Boxer. Computing deviations from convexity in polygons. *Pattern Recognition Letters*, 14:163–167, 1993.

6. M. Brady and A.L. Yuille. An extremum principle for shape from contour. *IEEE Trans. on Patt. Anal. and Mach. Intell.*, 6(3):288–301, 1984.

7. E. Bribiesca. Measuring 2-D shape compactness usng the contacct perimeter. *Pattern Recognition*, 33(11):1–9, 1997.

8. T.M. Chan. Approximating the diameter, width, smallest enclosing cylinder, and minimum-width annulus. *Int. J. Comput. Geometry Appl.*, 12(1-2):67–85, 2002.

9. J.S. Chang and C.K. Yap. A polynomial solution for the potato-peeling problem. *Discrete Comput. Geom.*, 1:155–182, 1986.

10. J. Chaudhuri, S.C. Nandy, and S. Das. Largest empty rectangle among a point set. *J. Algorithms*, 46(1):54–78, 2003.

11. D. Cremers, F. Tischhäuser, J. Weickert, and C. Schnörr. Diffusion snakes: Introducing statistical shape knowledge into the mumford-shah functional. *Int. Journal of Computer Vision*, 50(3):295–313, 2002.

12. M. de Berg, M. van Kreveld, M. Overmars, and O. Schwarzkopf. *Computational Geometry: Algorithms and Applications*. Springer-Verlag, 2nd edition, 2000.

13. M. Flickner *et al.* Image and video content: The QBIC system. *IEEE Computer*, 28(9):23–32, 1995.

14. S. Fischer and H. Bunke. Identification using classical and new features in combination with decision tree ensembles. In J.M.H. du Buf and M.M. Bayer, editors, *Automatic Diatom Identification*, pages 109–140. World Scientific, 2002.

15. A.W. Fitzgibbon, M. Pilu, and R.B. Fisher. Direct least square fitting of ellipses. *IEEE Trans. on Patt. Anal. and Mach. Intell.*, 21(5):476–480, 1999.

16. J. Flusser and T. Suk. Pattern recognition by affine moment invariants. *Pattern Recognition*, 26:167–174, 1993.

17. P. Franco, J.-M. Ogier, P. Loonis, and R. Mullot. A topological measure for image object recognition. In *Graphics Recognition*, volume 3088 of *Lecture Notes in Computer Science*, pages 279–290, 2004.

18. B. Gärtner. Fast and robust smallest enclosing balls. In *Algorithms – ESA*, volume 1643 of *LNCS*, pages 325–338, 1999.

19. B. Gärtner and S. Schönherr. Exact primitives for smallest enclosing ellipses. *Inf. Process. Lett.*, 68(1):33–38, 1998.

20. A. Ghali, M.F. Daemi, and M. Mansour. Image structural information assessment. *Pattern Recognition Letters*, 19(5-6):447–453, 1998.

21. G.H. Granlund. Fourier preprocessing for hand print character recognition. *IEEE Trans. on Computers*, 21:195–201, 1972.

22. W.G. Hayward. Effects of outline shape in object recognition. *Journal of Experimental Psychology: Human Perception and Performance*, 24:427–440, 1998.

23. M.L. Hentschel and N.W. Page. Selection of descriptors for particle shape characterization. *Part. Part. Syst. Charact.*, 20:25–38, 2003.

24. D.W. Jacobs. Robust and efficient detection of salient convex groups. *IEEE Trans. on Patt. Anal. and Mach. Intell.*, 18(1):23–37, 1996.

25. R. Kakarala. Testing for convexity with Fourier descriptors. *Electronics Letters*, 34(14):1392–1393, 1998.

26. V.V. Kindratenko. On using functions to describe the shape. *J. Math. Imaging Vis.*, 18(3):225–245, 2003.

27. M. Koprnicky, M. Ahmed, and M. Kamel. Contour description through set operations on dynamic reference shapes. In *Int. Conf. on Image Analysis and Recognition*, volume 1, pages 400–407, 2004.

28. B. Landau, L.B. Smith, and S. Jones. Object shape, object function, and object name. *Journal of Memory and Language*, 38:1–27, 1998.

29. L.J. Latecki, R. Lakämper, and U. Eckhardt. Shape descriptors for non-rigid shapes with a single closed contour. In *Proc. Conf. Computer Vision Pattern Recognition*, pages 1424–1429, 2000.

30. V.F. Leavers. Use of the two-dimensional radon transform to generate a taxonomy of shape for the characterization of abrasive powder particles. *IEEE Trans. on Patt. Anal. and Mach. Intell.*, 22(12):1411–1423, 2000.

31. L. Liu and S. Sclaroff. Deformable model-guided region split and merge of image regions. *Image and Vision Computing*, 22(4):343–354, 2004.

32. S. Loncaric. A survey of shape analysis techniques. *Pattern Recognition*, 31(8):983–1001, 1998.

33. S. Maitra. Moment invariants. *Proc. IEEE*, 67:697–699, 1979.

34. S.G. Mallat. A theory for multiresolution signal decomposition: the wavelet representation. *IEEE Trans. on Patt. Anal. and Mach. Intell.*, 11(7):674–693, 1989.

35. R.R. Martin and P.L. Rosin. Turning shape decision problems into measures. *Int. J. Shape Modelling*, 10(1):83–113, 2004.

36. D. McCallum and D. Avis. A linear algorithm for finding the convex hull of a simple polygon. *Inform. Process. Lett.*, 9:201–206, 1979.

37. A. Medvedeva and A. Mukhopadhyay. An implementation of a linear time algorithm for computing the minimum perimeter triangle enclosing a convex polygon. In *Canadian Conf. on Computational Geometry*, pages 25–28, 2003.

38. R. Mukundan and K.R. Ramakrishnan. *Moment Functions in Image Analysis – Theory and Applications*. World Scientific, 1998.

39. J. O'Rourke, A. Aggarwal, S. Maddila, and M. Baldwin. An optimal algorithm for finding minimal enclosing triangles. *J. Algorithms*, 7:258–269, 1986.

40. D.L. Page, A. Koschan, S.R. Sukumar, B. Roui-Abidi, and M.A. Abidi. Shape analysis algorithm based on information theory. In *Int. Conf. Image Processing*, volume 1, pages 229–232, 2003.

41. H.K. Pao and D. Geiger. A continuous shape descriptor by orientation diffusion. In *Proc. Workshop on Energy Minimization Methods in Computer Vision and Pattern Recognition*, volume 2134, pages 544–559. LNCS, 2001.

42. E. Rahtu, M. Salo, and J. Heikkila. Convexity recognition using multi-scale autoconvolution. In *Int. Conf. Pattern Recognition*, pages I: 692–695, 2004.

43. R.M. Rangayyan, N.M. Elfaramawy, J.E.L. Desautels, and O.A. Alim. Measures of acutance and shape for classification of breast-tumors. *IEEE Trans. on Medical Imaging*, 16(6):799–810, 1997.

44. J. Rigau, M. Feixas, and M. Sbert. Shape complexity based on mutual information. In *Int. Conf. on Shape Modeling and Applications*, pages 357–362, 2005.

45. A. Rosenfeld. Compact figures in digital pictures. *IEEE Trans. on Systems, Man and Cybernetics*, 4:221–223, 1974.

46. A. Rosenfeld. Measuring the sizes of concavities. *Pattern Recognition Letters*, 3:71–75, 1985.

47. P.L. Rosin. Ellipse fitting using orthogonal hyperbolae and Stirling's oval. *CVGIP: Graphical Models and Image Processing*, 60(3):209–213, 1998.

48. P.L. Rosin. Further five-point fit ellipse fitting. *CVGIP: Graphical Models and Image Processing*, 61(5):245–259, 1999.

49. P.L. Rosin. Measuring rectangularity. *Machine Vision and Applications*, 11:191–196, 1999.

50. P.L. Rosin. Shape partitioning by convexity. *IEEE Trans. on Systems, Man and Cybernetics*, part A, 30(2):202–210, 2000.

51. P.L. Rosin. Measuring shape: Ellipticity, rectangularity, and triangularity. *Machine Vision and Applications*, 14(3):172–184, 2003.

52. P.L. Rosin. Measuring sigmoidality. *Pattern Recognition*, 37(8):1735–1744, 2004.

53. P.L Rosin. Computing global shape measures. In C.H. Chen and P.S.-P. Wang, editors, *Handbook of Pattern Recognition and Computer Vision*, pages 177–196. World Scientific, 3rd edition, 2005.

54. P.L. Rosin and J. Hervás. Remote sensing image thresholding for determining landslide activity. *Int. J. Remote Sensing*, 26(6):1075–1092, 2005.

55. P.L. Rosin and J. Žunić. Measuring rectilinearity. *Computer Vision and Image Understanding*, 99(2):175–188, 2005.

56. L.K. Samuelson and L.B. Smith. They call it like they see it: Spontaneous naming and attention to shape. *Developmental Science*, 8(2):182–198, 2005.

57. M.H. Singer. A general approach to moment calculation for polygons and line segments. *Pattern Recognition*, 26(7):1019–1028, 1993.

58. H.I. Stern. Polygonal entropy: a convexity measure. *Pattern Recognition Letters*, 10:229–235, 1989.

59. G.T. Toussaint. Solving geometric problems with the rotating calipers. In *Proc. IEEE MELECON '83*, pages A10.02/1–4, 1983.

60. W.H. Tsai and S.L. Chou. Detection of generalized principal axes in rotationally symetric shapes. *Pattern Recognition*, 24(1):95–104, 1991.

61. R.C. Veltkamp and L.J. Latecki. Properties and performances of shape similarity measures. In *Conf. Data Science and Classification*, 2006.

62. A.D. Ventura, A. Rampini, and R. Schettini. Image registration by recognition of corresponding structures. *IEEE Trans. on Geoscience and Remote Sensing*, 28(3):305–314, 1990.

63. K. Voss and H. Süße. Invariant fitting of planar objects by primitives. *IEEE Trans. on Patt. Anal. and Mach. Intell.*, 19(1):80–84, 1997.

64. L. Wei, E. Keogh, and X. Xi. SAXually explicit images: Finding unusual shapes. In *Int. Conf. on Data Mining*, 2006.

65. I.T. Young, J.E. Walker, and J.E. Bowie. An analysis technique for biological shape. I. *Information and Control*, 25(4):357–370, 1974.

66. C.T. Zahn and R.Z. Roskies. Fourier descriptors for plane closed curves. *IEEE Trans. on Computers*, C-21:269–281, 1972.

67. D. Zhang and G. Lu. Review of shape representation and description techniques. *Pattern Recognition*, 37(1):1–19, 2004.

68. J. Žunić, L. Kopanja, and J.E. Fieldsend. Notes on shape orientation where the standard method does not work. *Pattern Recognition*, 39(2):856–865, 2006.

69. J. Žunić and P.L. Rosin. Rectilinearity measurements for polygons. *IEEE Trans. on Patt. Anal. and Mach. Intell.*, 25(9):1193–1200, 2003.

70. J. Žunić and P.L. Rosin. A new convexity measurement for polygons. *IEEE Trans. on Patt. Anal. and Mach. Intell.*, 26(7):923–934, 2004.

71. J. Žunić, P.L. Rosin, and L. Kopanja. On the orientability of shapes. *IEEE Trans. on Image Processing*, 15(11):3478–3487, 2006.